THE JOURNAL OF PHYSICAL CHEMISTRY C

Article

Cite This: J. Phys. Chem. C 2018, 122, 29386−29397

pubs.acs.org/JPCC

Nonenzymatic RNA Oligomerization at the Mineral−Water Interface: An Insight into the Adsorption−Polymerization Relationship

Hussein Kaddour,[†,¶,□] Selim Gerislioglu,[§] Punam Dalai,[†] Toshikazu Miyoshi,[†] Chrys Wesdemiotis,[†,§] and Nita Sahai*[,†,∥,⊥]

[†]Department of Polymer Science, 170 University Avenue, University of Akron, Akron, Ohio 44325, United States

[§]Department of Chemistry, [∥]Department of Geosciences, and [⊥]Integrated Bioscience Program, University of Akron, Akron, Ohio 44325, United States

Supporting Information

ABSTRACT: Nonenzymatic RNA polymerization, a major challenge in understanding the origins of life on early Earth, was previously achieved in the presence of montmorillonite clay and high magnesium concentrations (~75 mM), but the molecular interactions promoting ribonucleotide oligomerization remain unknown. High adsorption capacity of minerals is generally assumed to favor polymerization efficiency; however, this relationship was never shown. Here we examined the relationship between ribonucleotide adsorption affinity and the role of magnesium in the polymerization catalytic efficiency of minerals. Results showed that adsorption of the activated mononucleotide, 2-methylimadzolide of adenosine monophosphate (2-MeImPA), is approximately 10 times higher on zincite (ZnO) than on montmorillonite clay, but only montmorillonite acts as a catalyst for 2-MeImPA polymerization. In the presence of montmorillonite, oligomers formed even in pure water without any salts present. Attenuated total reflectance FTIR and cross-polarization-magic angle spinning ^{31}P NMR spectroscopy showed that 2-MeImPA mononucleotides adsorption on ZnO directly involves the phosphate moiety, making it unavailable for polymerization. In contrast, mononucleotides adsorbed on montmorillonite by weak amine interactions leaving the phosphate moiety available for polymerization. Thus, providing a favorable orientation of the monomer, rather than a high adsorption capacity, as well as providing a nanoconfined environment and outer-sphere complex formation with the nucleotide are requisite properties for a mineral to be catalytic to nucleotide polymerization.

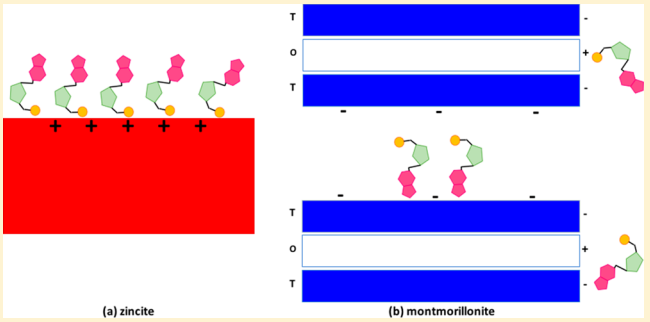

1. INTRODUCTION

One of the major challenges in the origins of life field is the nonenzymatic synthesis of RNA oligomers long enough to bear functionality.[1,2] In the absence of enzymes, minerals have long been proposed to have played the role of catalysts.[3] Pioneering work of James Ferris and co-workers at Rensselaer Polytechnic Institute for the past 30 years has demonstrated that montmorillonite clay promotes the nonenzymatic polymerization of activated RNA mononucleotides in the presence of magnesium or alkali cations.[4−19] Early work from the Ferris group also showed only short oligomers up to about 10- or 12-mers.[7,20] Long oligomers up to approximately 40-mers were subsequently claimed, based on gel electrophoresis results without mass spectrometry for confirmation,[10] but those results have not been reproducible and recently only short oligomers up to 9-mers were shown unambiguously.[18,21] Furthermore, the detailed molecular-level interactions at the mineral−organic interface responsible for the catalytic effect of montmorillonite on activated ribonucleotide polymerization remain unknown to date. Based on the results obtained for montmorillonite, it has been repeatedly hypothesized in the literature that the catalytic activity of minerals relies on their capacity to adsorb prebiotic organics,[22] with much attention given to the amount of adsorption or adsorption capacity of a mineral.[9,23,24] Adsorption is hypothesized to lead to the emergence of "surface organisms" or "surface metabolists".[25] While high adsorption capacity may be important for other reasons, such as protection of the RNA from degradation,[26] the assumed correlation of adsorption capacity to polymerization efficiency remains untested. Thus, most studies simply examine RNA monomer (ribonucleotide or ribonucleoside) adsorption but not the polymerization reaction.[27−38] Even these studies focus only on the simple mononucleotide whereas clay-catalyzed polymerization requires the activated mononucleotide. Conversely, other studies investigated the potential catalytic activity of various minerals (magnesite, calcite, dolomite, olivine, brucite, talc, montmorillonite, goethite, hematite, magnetite, siderite, galena, sphalerite, and chalcocite) to promote nonenzymatic RNA polymerization and found only montmorillonite to be catalytic,[13,20] but these studies did not

Received: October 22, 2018
Revised: November 20, 2018
Published: December 5, 2018

DOI: 10.1021/acs.jpcc.8b10288
J. Phys. Chem. C 2018, 122, 29386−29397

include a detailed investigation of the adsorption characteristics of the various minerals. Thus, a relationship between the adsorption capacity and the catalytic activity of minerals in promoting ribonucleotide polymerization has yet to be determined. From a surface chemistry standpoint, the apparently unique catalytic activity of montmorillonite is intriguing because montmorillonite and the nucleotides are both negatively charged at the optimal pH of polymerization (pH 7−8); hence, adsorption should be limited. This is probably the need for cations (Na^+, Mg^{2+}, Ca^{2+}) in the polymerization reaction in order to facilitate the coordination of the nucleotides to the mineral surface.[9]

Furthermore, not even all montmorillonites are excellent catalysts—the efficiency depends on the provenance of the clay, which reflects the extent of isomorphous chemical substitution in the crystal structure during the formation of the clay and on its treatment prior to the polymerization experiment by the so-called "Banin procedure".[16,39] These factors apparently affect the cation-exchange capacity and acid−base properties of the clay. Finally, most of the reported nonenzymatic RNA polymerization reactions on montmorillonite are slow (days) and the yields are low (<1%),[1] urging therefore the search for better catalysts from the plausible prebiotic mineral inventory.[18,21] An understanding of the montmorillonite-catalyzed polymerization mechanism would help to identify other minerals with potential catalytic activity.

In an attempt to identify the polymerization mechanism, the pH dependence of nucleotide adsorption and subsequent polymerization on three different montmorillonites was studied by Joshi and co-workers.[17] The authors investigated the role of each functional group of both the mineral and the nucleotide in the mechanism of adsorption. With these results, together with XRD data, it was proposed that polymerization is acid−base catalyzed, and a mechanism was proposed wherein a hydroxyl edge site of montmorillonite triggers the nucleophilic attack. This mechanism, however, does not address how the nucleotides are arranged at the mineral surface or what would be the active conformation of the monomer to trigger the nucleophilic attack.

Moreover, dissolved magnesium at concentrations of up to 50−75 mM is required for nonenzymatic RNA polymerization in the presence of montmorillonite as shown by Ferris and coworkers[6,16] or in the presence of a soluble RNA template.[40] This is much higher than the concentrations expected at the Earth's surface either prebiotically or on modern Earth.

The main goals of the present study were to shed light on any potential relationship between adsorption capacity and polymerization efficiency of various ribonucleotide monomers and to determine the adsorbed conformation of the monomers required for polymerization. We also investigated the effects of aqueous magnesium concentration on polymerization. In detail, we determined adsorption of the 2-methylimidazolide of 5′-adenosine monophosphate (2-MeImPA), as well as the polymerization of 2-MeImPA and of 3′,5′-cyclic adenosine monophosphate (3′,5-cAMP) (Figure S1). Cyclic nucleotide monomers generally accepted to be prebiotically plausible,[41,42] and 3′5′-cyclic guanosine monophosphate (cGMP) monomers have been found recently to polymerize nonenzymatically in water[43] and under dry conditions at moderate temperatures (50−80 °C).[44]

Adsorption and polymerization were examined on montmorillonite, which is known to promote polymerization, and on zincite, which shows strong affinity for 5′-AMP based on preliminary results in our laboratory. The conformation of the adsorbed molecule is expected to be a key determinant of polymerization efficiency because the phosphate moiety should be available for polymerization. Conformation of adsorbed monomer was determined by Fourier transform infrared (FTIR) and solid state nuclear magnetic resonance (ss-NMR) spectroscopy. These spectroscopic methods have been used previously for probing the structure of mononucleobases and mononucleosides[35,45] but rarely that of adsorbed mononucleotides.[30,46−48]

2. MATERIALS AND METHODS

2.1. Materials. All chemical reagents used in the synthesis of activated nucleotides were purchased either from Sigma-Aldrich (Saint Louis, MO) or from Fisher Scientific (Waltham, MA), except 3′,5′-cyclic AMP free acid form (Biolog-Life Science Institute, Germany). Zincite (ZnO, 99.999%, trace metal basis) was purchased from Sigma-Aldrich. Natural montmorillonite (Wyoming, Volclay SPV-200) was purchased from the American Colloid Company (Troy, IN). All water used was ultrapure (18 MΩ-cm) (Nanopore UV, Barnstead, NH).

2.2. Mineral Characterization. Minerals were characterized as described previously in detail.[49] The identity of both minerals was confirmed by X-ray diffraction (Ultima IV Rigaku, DE). Their specific surface areas were determined by multipoint N_2 gas adsorption fit to BET isotherm (Micromeritics, GA). Particle sizes and crystal morphology were estimated by transmission electron microscopy (TEM, JSM-1230, ∼120 kV, JEOL, MA). Two microliters of 0.1 mg·mL^{-1} of each mineral suspension was placed on 300-mesh copper grids coated with Formvar/carbon film and dried in air. Isoelectric points (IEP) were determined by measuring the zeta potential of mineral suspensions (1 mg·mL^{-1}) as a function of pH in ultrapure water and identifying the point of zero potential (Zetasizer NanoSeries ZS, Malvern Instruments, U.K.).[49] Catalytic montmorillonite was prepared according to the Banin procedure[39] as described by Joshi et al.,[16] which involves titrating the H^+-form of the clay with 0.1 M NaOH to pH 8.

2.3. Synthesis of 2-MeImPA. The 2-methylimidazolide of 5′-adenosine monophosphate (5′-AMP) was prepared following the original published procedure[50] with slight modifications adapted from Joshi et al.[15] In detail, 5′-AMP monohydrate (611 mg) and 2-methylimidazole (1.8 g) were dissolved in 10 mL of anhydrous dimethylformamide (DMF), and the solvent was evaporated to dryness in a rotary evaporator (Heidolph, HeiVap, Germany). The evaporation was repeated twice with anhydrous DMF to remove residual water, and the flask was kept overnight in a vacuum desiccator. The residue was again dissolved in 10 mL of anhydrous DMF and stirred with triphenylphosphine (1.2 g), 2,2′-dithiodipyridine (1.4 g), and triethylamine (0.9 mL) at room temperature for 16 h. The incubation duration was increased from 4 to 16 h to maximize the yields. The resulting product was precipitated in a solution of anhydrous diethyl ether (300 mL), acetone (99.5% pure, 200 mL), and sodium perchlorate (3.5 g), washed with 1:1 acetone/ether solution, and then washed with ether alone until the yellowish color disappeared, and then ether was finally dried in a vacuum desiccator overnight. The formation of 2-MeImPA was confirmed by electron spray ionization mass spectrometry analysis (ESI-MS), and its purity (∼97 ± 3%) was determined by reverse phase HPLC on a

DOI: 10.1021/acs.jpcc.8b10288
J. Phys. Chem. C 2018, 122, 29386−29397

Kinetex biphenyl column (Phenomenex) (Figure S2). The activated nucleotide was used without purification.

2.4. Adsorption Isotherms. Adsorption of 2-MeImPA on minerals was measured through batch experiment with 10 mg·mL^{-1} mineral particle loading and a nucleotide concentration ranging from 0 to 4 mM in ultrapure water. Reaction mixtures were prepared in 1.5 mL eppendorf tubes from stock solutions of 10 mM nucleotide and stock suspensions of 20 mg·mL^{-1} of mineral, prepared in water. Accurate pipetting was assured using electronic multichannel micropipettes (E1 Cliptip, Thermo Scientific) to achieve maximum reproducibility of results. Samples were briefly vortexed and incubated at room temperature for 24−48 h with occasional vortexing. Samples were then centrifuged at 13 300 rpm (Accuspin Micro 17, Fisher Scientific, Waltham, MA) for 25 min at 25 °C, and the supernatants were collected. The UV−vis absorbance of the supernatant solutions was measured using a NanoDrop 2000c spectrophotometer (Thermo Fisher Scientific, Waltham, MA). Error bars represent standard deviation of triplicate samples. The experiment was repeated three times in triplicate.

2.5. Polymerization Reactions. For polymerization of 2-MeImPA, the procedure was adapted from Joshi et al.[15] In 1.5 mL eppendorf tubes, 15 μL of 100 mM 2-MeImPA stock solution (freshly prepared) was mixed with 10 μL of 10× polymerization buffer (2 M NaCl, 0.75 M $MgCl_2$) and diluted with water to reach final concentrations of 200 mM NaCl, 75 mM $MgCl_2$ (polymerization buffer), and 15 mM 2-MeImPA, in a reaction volume of 100 μL. To this reaction, 5 ± 0.3 mg of mineral was added, yielding a mineral loading of 50 mg·mL^{-1}. The mixture was vortexed briefly and kept at room temperature for 3 days. It is worthwhile to mention that experiments where pH was adjusted to 8 by the presence of 0.2 M buffer (HEPES or bicine) were conducted, but only a monomer−buffer covalently bonded complex was obtained, and apparently this complex inhibited the formation of oligomers, as evidenced by the results of ESI-MS analysis (Figure S3). Samples without minerals and/or without any salts were similarly prepared.

RNA monomer and oligonucleotides were extracted prior to their identification as follows. At the end of the above-described polymerization reaction, the samples were centrifuged at 4000 rpm (Accuspin Micro 17, Fisher Scientific, Waltham, MA) for 5 min at 25 °C, and the supernatants were collected. To the mineral pellet, 200 μL of extraction solution (0.1 M EDTA, pH 11) was added, and the samples were thoroughly vortexed for at least 1 h. The extraction was repeated twice, the supernatants from each extraction cycle were combined, and the volume was adjusted to 1 mL with water. The pH was adjusted to 4 with ∼20 μL of 1 M perchloric acid, and the sample was incubated at 37 °C for 1 h to hydrolyze the unreacted 2-MeImPA. Samples were finally filtered through cellulose acetate centrifuge tube filters (SpinX, Costar, Corning, NY) with a pore size of 0.22 μm.

3′,5′-Cyclic AMP H^+-form was polymerized in dry conditions following the method of Morasch et al.[44] Briefly, 15 mM of 3′,5′-cyclic AMP was incubated in the presence and absence of minerals (50 mg·mL^{-1}) and in the presence and absence of polymerization buffer (200 mM NaCl, 75 mM $MgCl_2$) in a 200 μL reaction volume, and the mixture was incubated under vacuum (Eppendorf, Vacufuge Plus) at 60 °C for 16 h. RNA was extracted from the minerals with 0.1 M EDTA pH 11 (200 μL, 1 h, 3 times), and the extracts were filtered.

2.6. HPLC Analysis. HPLC analysis was performed using a Shimadzu Nexera 2 system equipped with a Photo Diode Array UV/vis detector. The polymerization products were separated on a Dionex DNAPac-200 RS, 4 μm (4.6 × 250 mm^2) analytical anion exchange column, using a gradient of 0−0.2 M $NaClO_4$ with 2 mM Tris at pH 8, a method adapted from Joshi et al.[15] All samples were filtered through 0.22 μm cellulose acetate filters (SpinX, Costar) prior to analysis. Analysis of the 2-MeImPA was performed on a Kinetex Biphenyl 2.6 μm, 100 Å column, 100 × 4.6 mm (Phenomenex) using a mobile phase of H_2O/MeCN (98:2) acidified with 0.1% TFA at a flow rate of 1 mL·min^{-1}. Both separations were carried out at 40 °C.

2.7. Mass Spectrometry. Matrix-assisted laser desorption/ionization mass spectrometry (MALDI-MS) experiments were performed on a Bruker Ultraflex III MALDI tandem time-of-flight (TOF/TOF) mass spectrometer (Bruker Daltonics, Billerica, MA) equipped with a Nd:YAG laser emitting at 355 nm. All samples were analyzed before and after desalting using a "ziptip." The samples were desalted using C_{18}-Millipore Ziptips (Sigma-Aldrich, St Louis, MO) according to the manufacturer's guidelines. 6-Aza-2-thiothimidine (ATT) (99%; Sigma-Aldrich, St. Louis, MO) served as matrix. The matrix solution was prepared in H_2O/MeCN (50:50, v/v) at 2 mg·mL^{-1} concentration. The matrix and sample solutions were mixed in the ratio 5:1 (v/v), and 0.5−1.0 μL of the final mixture was applied to the MALDI target plate and allowed to dry at ambient room conditions before spectral acquisition at negative ion mode. This sample preparation protocol with or without desalting led to the formation of $[M - H]^-$ or $[M + mNa - nH]^-$ ($n - m = 1$) ions, respectively, where M corresponds to the mass of the compound of interest and − H indicates that the compound was ionized by deprotonation to form an anion. Spectral acquisition was carried out at reflectron mode, and ion source 1 (IS 1), ion source 2 (IS 2), source lens, reflectron 1, and reflectron 2 potentials were set at 25.03, 21.72, 9.65, 26.32, and 13.73 kV, respectively. The MALDI-MS data were analyzed using Bruker's flexAnalysis v3.3 software.

Electrospray ionization MS analyses were carried out by Bruker HCT Ultra II quadrupole ion trap mass spectrometer (Bruker Daltonics, Billerica, MA) equipped with ESI source. Samples were diluted to 1 μg·mL^{-1} in H_2O/MeCN (50:50, v/v). The sample solutions were injected into the ESI source by direct infusion, using a syringe pump, at a flow rate of 3 μL·min^{-1}. The tip of the ESI needle was grounded, and the entrance of the capillary, through which ions enter in the vacuum system of the mass spectrometer, was held at 3.5 kV. The pressure of the nebulizing gas (nitrogen) was set at 10 psi, and the flow rate and temperature of the drying gas (nitrogen) were 8 L·min^{-1} and 300 °C, respectively. Data collection was performed on negative ion mode. The ESI-MS data were analyzed using Bruker's DataAnalysis v4.0 software.

2.8. ATR-FTIR Spectroscopy. Four millimoles of 2-MeImPA or 5′-AMP-Na in 15 mL of pure water was mixed with 150 mg of zincite. Because of weak adsorption, 10 mM of 2-MeImPA in 15 mL pure water was mixed with 150 mg of Banin-treated montmorillonite. All suspensions were incubated on a rotary shaker (SB3 Rotator, Stuart, Staffordshire, U.K.) overnight. Samples were then centrifuged at 10 000 rpm for 15 min, and supernatants were discarded. The pellets obtained were frozen with liquid nitrogen and dried using lyophilizer (FreeZone 2.5, Labconco, Kansas City, MO) for 24 h. Measurements were performed with a Thermo Nicolet 380

DOI: 10.1021/acs.jpcc.8b10288
J. Phys. Chem. C 2018, 122, 29386−29397

FTIR instrument (Thermo Fisher Scientific, Waltham, MA). Each spectrum was recorded in ATR mode with the use of an ATR Smart Orbit between 500 and 4000 cm^{-1} range with 64 scans with a resolution of 4 cm^{-1} at room temperature.

2.9. NMR Spectroscopy. Solid-state magic angle spinning (MAS) NMR experiments were performed on a Bruker Avance 300 instrument with resonance frequencies of 121.5 and 300.1 MHz for ^{31}P and ^{1}H, respectively. A 7 mm double-resonance probe was used for cross-polarization magic angle spinning (CPMAS) experiment at a MAS frequency of 4 kHz. The radio frequency field strength was set to 62.5 kHz for both ^{1}H and ^{31}P channels. The $^{1}H-^{31}P$ CP contact time was set to 2 ms. ^{1}H two-phase pulse modulation (TPPM) with a field strength of 62.5 kHz was applied during the ^{31}P signal acquisition time of 10 ms. Accumulation numbers of signals (NS) and recycle delay (RD) were varied depending on the sample. For 2-MeImPA, the CP-MAS conditions were the following: 2-MeImPA standard, NS = 512, RD = 14 s; zincite, NS = 4000, RD = 3 s; montmorillonite, NS = 500 000, RD = 500 ms; The CP static conditions were the following: 2-MeImPA standard, NS = 2048; zincite = 16 000, RD = 3 s. Analysis was performed on samples prepared similarly as for FTIR. Briefly, 4 mM of 2-MeImPA or 5′-AMP-Na in 15 mL of pure water was mixed with 150 mg of zincite or Banin-treated montmorillonite, and the suspensions allowed to equilibrate overnight with end-over-end rotation. Samples were then centrifuged at 10 000 rpm for 15 min, and the pellets obtained were freeze-dried using lyophilizer for 24 h.

3. RESULTS AND DISCUSSION

3.1. Adsorption Isotherms. The adsorption of 2-MeImPA mononucleotide on zincite and montmorillonite in water was examined as a function of increasing monomer concentration at room temperature (Figure 1). Adsorption on zincite was greater than on montmorillonite at all equilibrium concentrations (C_{eq}) of the monomer up to a factor of 10× greater at C_{eq} = 2 mM. No adsorption maximum was obtained within the concentration range examined.

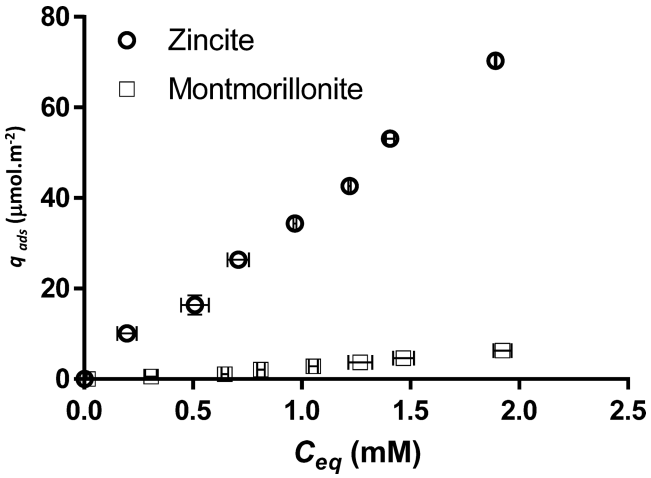

Figure 1. Adsorption of activated nucleotide 2-MeImPA (A) on zincite (circles) and montmorillonite (squares) in ultrapure water. Mineral loading = 10 mg·mL^{-1}. Isotherms are reported as mass adsorbed, q_e (μmol.m^{-2}), as a function of the equilibrium solution concentration, C_{eq}. The error bars represent the standard deviation from the mean of three replicate samples.

3.2. Nonenzymatic RNA Polymerization. Polymerization of 2-MeImpA and 3′,5′-cAMP mononucleotides was investigated on zincite and montmorillonite under two different experimental systems, representing two different schools in the origins of life literature: the Ferris school and the Di Mauro school.[4,5,7−16,18−20,43,51] In the first system, the experimental conditions consisted of a mixture of 10 mM 2-MeImPA, 50 mg·mL^{-1} mineral loading, 200 mM NaCl, and 75 mM $MgCl_2$, which was incubated for 3 days at room temperature (see Materials and Methods).[16] HPLC analysis revealed the presence of oligomers up to only trimers in the presence of ZnO, which was similar to the control system without minerals present (Figure 2a, b). Longer oligomers up to octamers were obtained in the presence of montmorillonite (Figure 2c).

MALDI-MS analysis (Figure 2d−f) was carried out to confirm the HPLC results. The theoretical and the experimental mass-to-charge ratio (m/z) values of oligomer ions from 2-mer to 8-mer are summarized in Table S1. Again, only trimers were detected from the ZnO system similar to the control system (Figure 2d, e), whereas longer oligomers were observed with montmorillonite (Figure 2f; Table S1). Peaks corresponding to the theoretical m/z of oligomers up to 6-mer were identified from montmorillonite samples. Two oligomeric ion series were observed in the MALDI-MS spectrum (Figure 2f). The a_n ion series corresponds to linear oligomers (from 2-mer to 6-mer) of 2-MeImPA, whereas the a_n* series indicates ions with loss of one water molecule (a_n − 18 Da), showing the presence of oligomers that contain one cyclic monomer. Note that peaks for longer oligomers (7-mer and 8-mer) were found in the samples that had not been purified by "zip-tipping" (Figure S4). The absence of the 7-mer and 8-mer in the zip-tipped sample (Figure 2f) is explained by their low abundance and low recovery of these oligomers during the ziptip process.

MALDI-MS analysis of the nonziptipped sample showed aggregates of oligomers with differing lengths and multiple sodium adducts because of high salt concentration in the sample (Figure S4). Formation of such aggregates and salt adducts also resulted in a more convoluted spectrum. However, zooming in to the higher m/z values (2000−2900 m/z) allowed the identification of 7- and 8-mers (Figure S4). The amount of sodium adducts are indicated as a superscript on each oligomer ion observed in the spectrum of the nonziptipped samples. For example, the ion observed at 2057.84 m/z, a_6^{3Na}, corresponds to the 6-mer with three Na^+ adducts ($[M + 3Na - 4H]^-$ (Figure S4). The presence of the ion series, which is 18 Da higher than a_n ions (labeled as b_n), showed the formation of aggregates by noncovalent interaction of two oligomers. For example, the ion observed at 2075.88 m/z corresponds to an aggregate of two oligomers with a total number of 6 monomers and 3 Na^+ adducts.

In the second polymerization system following Di Mauro and co-workers,[43,44,52] the H^+-form of the cyclic monomer (15 mM 3′,5′-cAMP) was incubated in dry conditions in the absence or presence of 50 mg·mL^{-1} montmorillonite and zincite at 60 °C for 16 h (see Materials and Methods). Controls with and without salts (200 mM NaCl, 75 mM $MgCl_2$) were also tested. No polymers above dimers could be detected by HPLC (Figure S5) or MALDI-MS (Figure S6). The structure of these dimers, however, cannot be ascertained definitively from the mass spectra alone, since covalently- and noncovalently bound dimers of 3′,5′-cAMP have the same empirical formula and mass. Therefore, the ion observed at 657

DOI: 10.1021/acs.jpcc.8b10288
J. Phys. Chem. C 2018, 122, 29386−29397

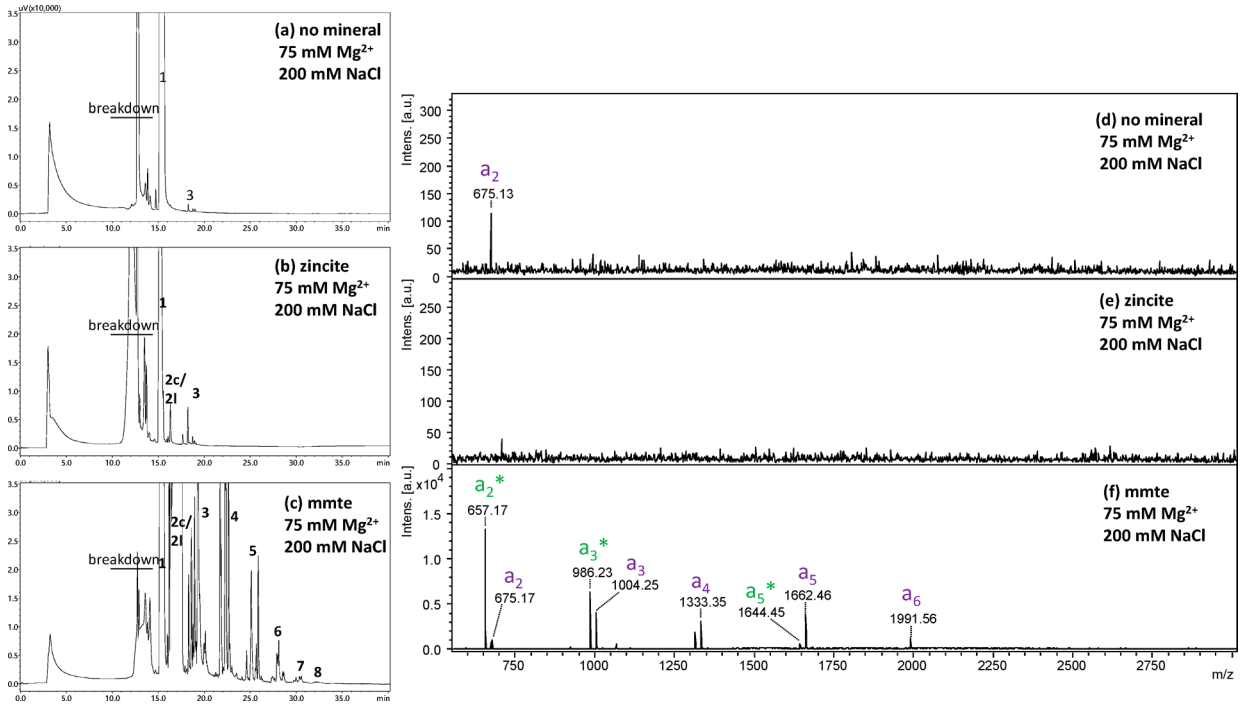

Figure 2. Nonenzymatic polymerization of 2-MeImPA in the presence of 200 mM NaCl and 75 mM $MgCl_2$ (classical polymerization buffer). (a)−(c) Anion-exchange HPLC chromatograms and (d)−(f) MALDI-TOF MS spectra. (a, d) In the absence of mineral; (b, e) in the presence of zincite; and (c, f) in the presence of Banin-treated montmorillonite. Mineral loading = 50 mg.mL^{-1}. In the HPLC chromatograms, "breakdown" refers to the monomer hydrolysis products. The numbers refer to the *n*-mer oligomer and 2c and 2l refer to the cyclic dimer and the linear dimer, respectively (see Figure S1 for structures). In the MALDI-TOF MS spectra, a_n is the ion series corresponding to oligomers with *n*-mers. The ions that are labeled with asteriks (a_n*) correspond to oligomers with a water loss. All of the ions observed in the spectra are deprotonated, $[M - H]^-$.

m/*z* could also correspond to a noncovalently associated cluster of 2 monomers (Figure S7).[21] The difference between the previously reported polymerization of cyclic monomers and the present study may be because the original authors used 3′,5′-cGMP whereas 3′,5′-AMP is used here. The absence of polymerization even in the presence of montmorillonite indicates that different mechanistic pathways are involved in the polymerization of the activated linear (2-MeImPA) and the cyclic (3′,5′-cAMP) monomers.[43,44,51,52]

Other experimental conditions consisting of 1-week incubation time and hydration/dehydration cycles with 3′,5′-cAMP were also tested (Figure S8). Only a peak of 313 *m*/*z* was dominant, corresponding to a ribosyl-pyrophosphate resulting from RNA dipurination at acidic conditions and high temperature, a finding that has been previously reported.[53] However, no oligomers were detected, in contrast to previous reports.[43,44]

3.3. Effect of Mg^{2+} Concentration on Polymerization. The catalytic efficiency of zincite and montmorillonite to promote 2-MeImPA polymerization was assessed in pure water, at Mg^{2+} concentrations of 10 and 100 mM $MgCl_2$, and in polymerization buffer (75 mM Mg^{2+} and 200 mM NaCl) on montmorillonite and zincite (Figures 3 and 4). The HPLC chromatograms (Figure 3) of the systems in pure water showed that montmorillonite catalyzes the polymerization up to pentamers (Figure 3c) while polymerization did not exceed trimers in the presence of zincite (Figure 3b). The HPLC chromatograms (Figure 4 a−d) and the MALDI-TOF spectra (Figure 4 e−h) at various Mg^{2+} concentrations show up to tetramers in pure water (Figure 4a, e) and slightly longer oligomers of up to about 5-mers or 7-mers in the presence of 10 mM Mg^{2+} (Figure 4b, f). However, further increasing the Mg^{2+} concentration up to 100 mM (Figure 4c, g) or the presence of the classical polymerization buffer (Figure 4d, h) does not significantly improve catalytic efficiency, yielding up to 8-mers. Interestingly, it was also observed that up to tetramers are formed at 100 mM Mg^{2+} in the absence of any mineral but not at lower (10 mM Mg^{2+}) concentration (Figure S9).

In summary, the results presented above demonstrated that Mg^{2+} is not essential for the formation of at least short oligomers of activated, linear monomer (2-MeImPA) and that montmorillonite is a better catalyst than zincite, even though the latter was found to have a much higher adsorption capacity.

Taken together, the results presented above indicate that the amount of adsorbed nucleotide is not the determining factor in the polymerization catalytic efficiency of a mineral. This suggests that the orientation of the nucleotides on the surface is a more important factor. In order to gain information concerning the binding conformation of nucleotides to the minerals and to correlate this binding information to the polymerization efficiency of the corresponding mineral, ATR-FTIR and ^{31}P ssNMR spectroscopy was performed for 2-MeImPA adsorbed on zincite and montmorillonite.

3.4. Adsorbed Monomer Conformation by ATR-FTIR Analysis. The FTIR spectra were interpreted based on band assignments for nucleobase, nucleoside, and nucleotides in solution as reported previously in the literature.[36,54−60] The bands between ∼1000 and 1180 cm^{-1} correspond to PO_4 bands of the mononucleotide (Figure 5). These bands overlap to some extent with the ribose bands between 960 and 1100 cm^{-1}. Bands corresponding to the nucleobase ring occur at ∼1580−1604 cm^{-1}, and the amine group appears at ∼1649 cm^{-1}. The spectrum on ZnO shows that the bands

DOI: 10.1021/acs.jpcc.8b10288
J. Phys. Chem. C 2018, 122, 29386−29397

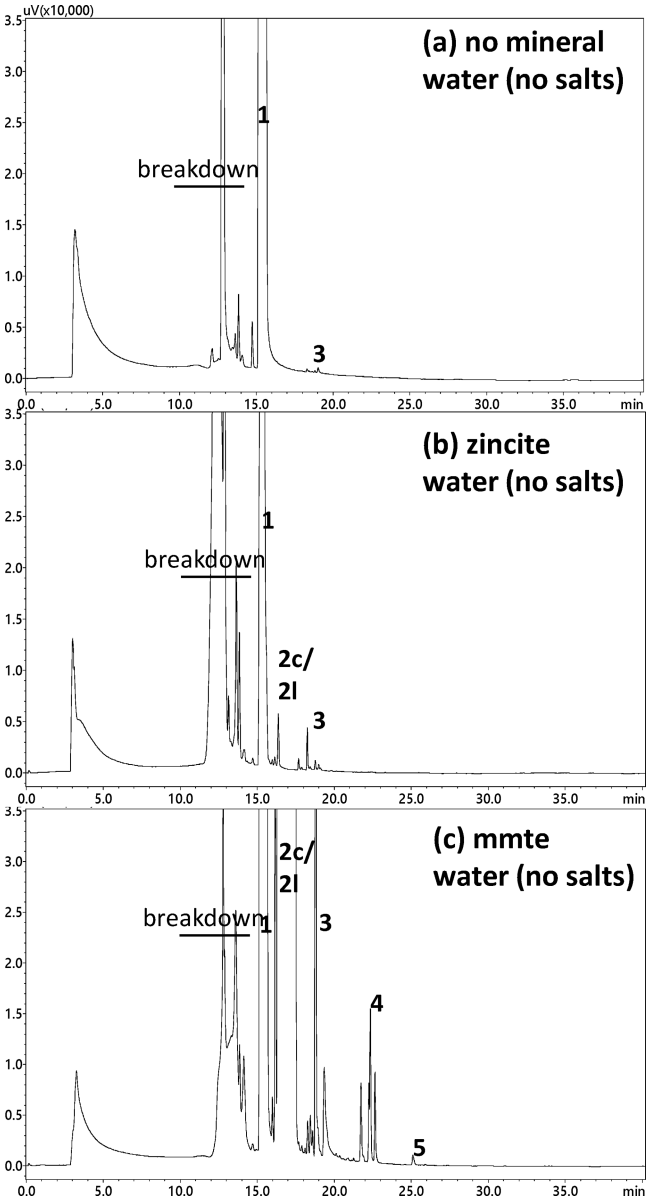

Figure 3. Anion-exchange HPLC chromatograms of nonenzymatic polymerization of 2-MeImPA in water (no salts present). (a) In the absence of mineral; (b) in the presence of zincite; and (c) in the presence of Banin-treated montmorillonite; the corresponding MALDI-TOF spectrum is shown in Figure 4a. Mineral loading = 50 mg·mL^{-1}. Breakdown refers to the monomer hydrolysis. The numbers refer to the *n*-mer oligomer, and 2c and 2l refer to the cyclic dimer and the linear dimer, respectively (see Figure S1 for structures).

corresponding to the phosphate group of the nucleotide are significantly altered upon adsorption to zincite, whereas the band assigned to the amine group is not affected. This suggests an inner-sphere complex between the phosphate moiety of the nucleotide monomer and the zinc atom of the zincite surface. If there were an outer-sphere complex in which the nucleotide is separated from the surface by an intervening water molecule, then the phosphate band would not have been shifted significantly.

The spectrum of montmorillonite shows broad bands at 900−1100 cm^{-1} corresponding to the Si−O−Si framework (Figure 5). These bands overlap the phosphate and ribose bands of the ribonucleotide. Interestingly, the ∼1649 cm^{-1} band of the ribonucleotide is shifted to 1634 cm^{-1} upon adsorption to montmorillonite clay indicating interaction of the amine group with the surface, indicating a H-bonded interaction.

Thus, the activated monomer interacts strongly by the phosphate group on zincite forming an inner-sphere surface complex and weakly through the amine group on montmorillonite forming an H-bonded complex.

3.5. Adsorbed Monomer Conformation by ssNMR Analysis. The NMR chemical shift interaction is characteristic in terms of the shielding effect of electron clouds surrounding the nucleus. Hence, anisotropic and isotropic chemical shifts are very sensitive to specific intermolecular interactions and environments surrounding target nuclei. ^{31}P CP NMR spectra of 2-MeImPA corresponding to magic angle spinning conditions (Figure 6a) show the nucleotide standard (bottom), adsorbed on zincite (middle) and adsorbed on montmorillonite (top). The 2-MeImPA standard sample has very intense signals. Interestingly, 2-MeImPA adsorbed on zincite also provided relatively strong ^{31}P signals, whereas the signal was very weak on montmorillonite and took 20−30 times larger accumulations than those on zincite. The CPMAS spectra of 2-MeImPA on montmorillonite took about 2 days to collect. The isotropic chemical shift trend for 2-MeImPA in bulk state (−9.5 ppm), adsorbed on montmorillonite (−0.5 ppm) and adsorbed on zincite (2.5 ppm), showed increasingly positive values. These chemical shift trends suggest stronger interactions between phosphate and the zincite surface than those between phosphate and the montmorillonite surface.

^{31}P NMR spectra collected under static conditions are shown for 2-MeImPA in Figure 6b for the standard (bottom) and adsorbed on zincite (top). In the standard, the chemical shift anisotropy (CSA) principle values (σ_{11}, σ_{22}, σ_{33} = 103, 16, −147 ppm) are largely different from those of 2-MeImPA adsorbed on zincite (σ_{11}, σ_{22}, σ_{33} = 63, −16, −35 ppm). This fact, again, suggests strong interaction between phosphate and surface of zincite. Note that very weak adsorption of 2-MeImPA on the surface of montmorillonite does not allow us to measure CSA pattern within a reasonable time period.

3.6. Relating Adsorption Capacity, Adsorbed Conformation, and Polymerization Efficiency. The primary focus of the present study was not to achieve long oligomers but to elucidate relationships between adsorption capacity, conformation of the adsorbed monomer, and polymerization catalytic efficiency of the minerals, if any. Zincite adsorbed up to 10× as much nucleotide as did montmorillonite under the present experimental conditions. However, polymerization efficiency was lower or absent on zincite. The present results are consistent with a body of results in the literature. For example, it was shown by Daniel and co-workers[33,37] that another clay mineral, nontronite, adsorbs twice as much nucleic acids as montmorillonite, but, in another earlier study, nontronite was found to show little or no catalytic activity compared to montmorillonite in RNA polymerization.[13]

In order to understand the adsorption capacity trends, we consider the surface charge characteristics of the two minerals. The isoelectric point (IEP) of zincite is ∼8.4,[49] so the surface is positively charged in water. Adsorption of the negatively charged nucleotide is, therefore, expected. Based on the crystal structure of ZnO, about 9 Zn sites per nm^2 of the ZnO surface can be estimated. Assuming adsorption of one nucleotide per surface Zn atom and complete surface coverage, the apparent maximum adsorption capacity on zincite translates to ∼50

DOI: 10.1021/acs.jpcc.8b10288
J. Phys. Chem. C 2018, 122, 29386−29397

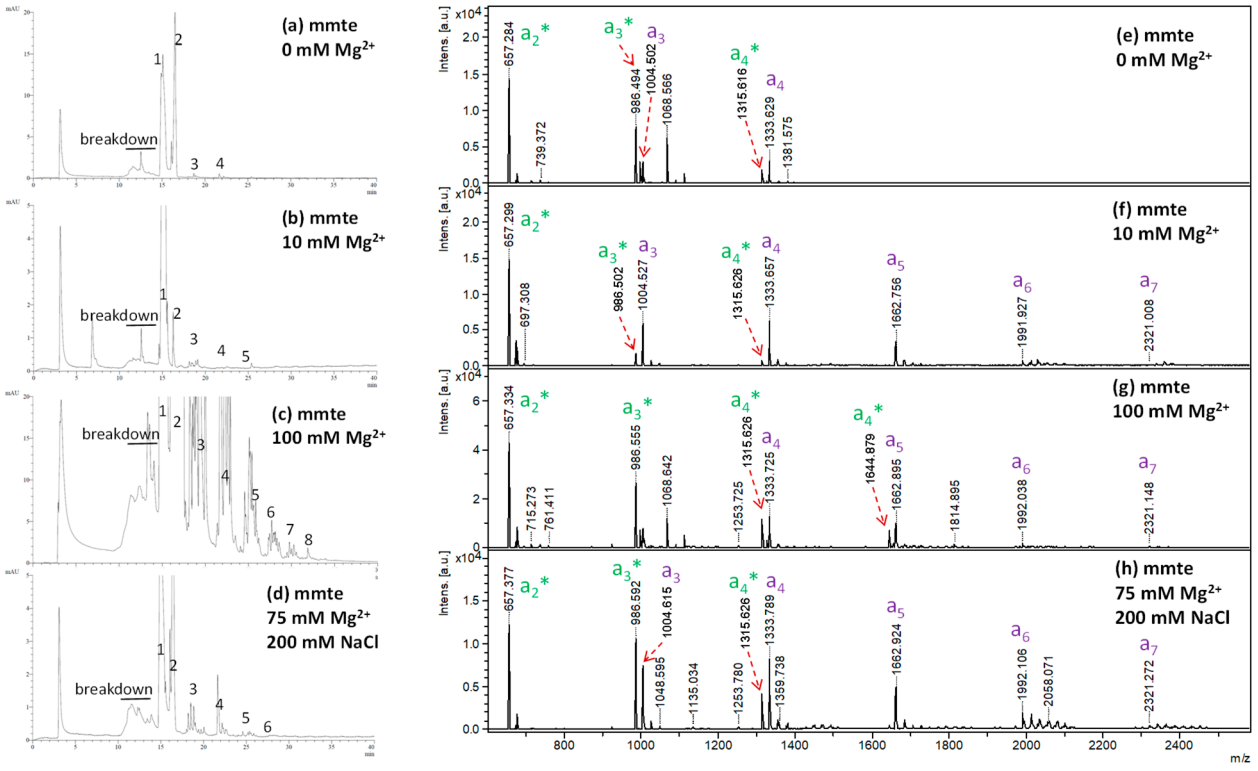

Figure 4. Anion-exchange HPLC chromatograms (a–d); MALDI-TOF spectra (e–h) of 2-MeImPA reacted in the presence of Banin-treated montmorillonite at various concentrations of Mg^{2+}: (a, e) 0 mM Mg^{2+}; (b, f) 10 mM Mg^{2+}; (c, g) 100 mM Mg^{2+}; and (d, h) 75 mM Mg^{2+} and 200 mM NaCl. Mineral loading = 50 mg.mL^{-1}.

molecules of nucleotide per nm^2 of zincite or roughly 4–5 layers of monomers.

In contrast, the negatively charged surface of montmorillonite (IEP ∼ 2.5[49]) is expected to repel the monomer. Yet, a small amount of adsorption is seen, presumably due to weak van der Waals and H-bonding interactions as indicated by the spectroscopic results. Some adsorption may also occur by the formation of Mg^{2+}–2MeImPA surface complexes. The present results show that adsorption of negatively charged nucleotides increases as the mineral surface charge becomes more positive suggesting a major contribution from electrostatic forces in controlling the adsorption capacity of a mineral. Since adsorption capacity is not the factor controlling polymerization catalytic efficiency of the minerals, the conformation of the adsorbed nucleotides is considered next.

The FTIR and ssNMR data indicate that the phosphate moiety of the nucleotide is strongly attracted to the metal cation surface sites on positively charged surfaces, leading to covalent bond formation as seen for zincite here, and well-established in the literature for other positively charged minerals, such as goethite (α-FeOOH) and gamma-alumina (γ-Al_2O_3).[49] The spectroscopic analyses also reveal that the phosphate moiety does not interact strongly with the negatively charged montmorillonite surface. This result indicates that van der Waals interactions or H-bonding between the surface −OH sites and nucleobase or amine moieties contribute, albeit weakly, to adsorption on negatively charged mineral surfaces. Our result is consistent with those from a recent molecular dynamics simulation, which showed that the amine group and the nucleobase in an activated ribonucleotide are oriented toward the silicate tetrahedral plane in the interlayer sites.[61]

Based on surface complexation model fits to a comprehensive set of adsorption data obtained over a range of pH and surface loadings conditions, it was previously concluded that nucleotides adsorb on swelling clays such as montmorillonite and nontronite by two mechanisms depending on the pH.[33,37] At low pH, it was proposed that nucleotides adsorb to the octahedral layer of clay at >FeOH or >MgOH edge sites via phosphate forming an inner-sphere monodentate surface complex and by ion exchange in the interlayer sites. At higher pHs, which is relevant to the pH 8 of the present study, Daniel and co-workers[30,37] proposed that nucleotides bind by forming bidentate outer-sphere complexes at >FeOH or >MgOH edge sites through the phosphate group. If such outer-sphere complexes do form, spectroscopy would not capture it; hence, our study does not identify such complexes. Conversely, the previous studies of Daniel and co-workers[30,37] are based solely on model fits to bulk adsorption data without any spectroscopic analysis, so they may have missed the presence of interlayer adsorption of nucleotides at high pH as shown by our FTIR data because it is a weak adsorption. Thus, it is likely that both interlayer adsorption of nucleotides by interaction between the nucleobase and interlayer sites of montmorillonite as shown here as well as outer-sphere complexation via the phosphate group to >FeOH or >MgOH edge sites at the octahedral layer of montmorillonite are occurring.

In summary, despite a much smaller adsorption capacity, polymerization on montmorillonite is much more efficient than on zincite because of the conformational differences of the adsorbed activated mononucleotide between the two minerals.

3.7. Model for Catalysis of Nucletoide Polymerization. Based on the data obtained in our study, a model for the nonenzymatic polymerization on minerals is proposed

DOI: 10.1021/acs.jpcc.8b10288
J. Phys. Chem. C 2018, 122, 29386–29397

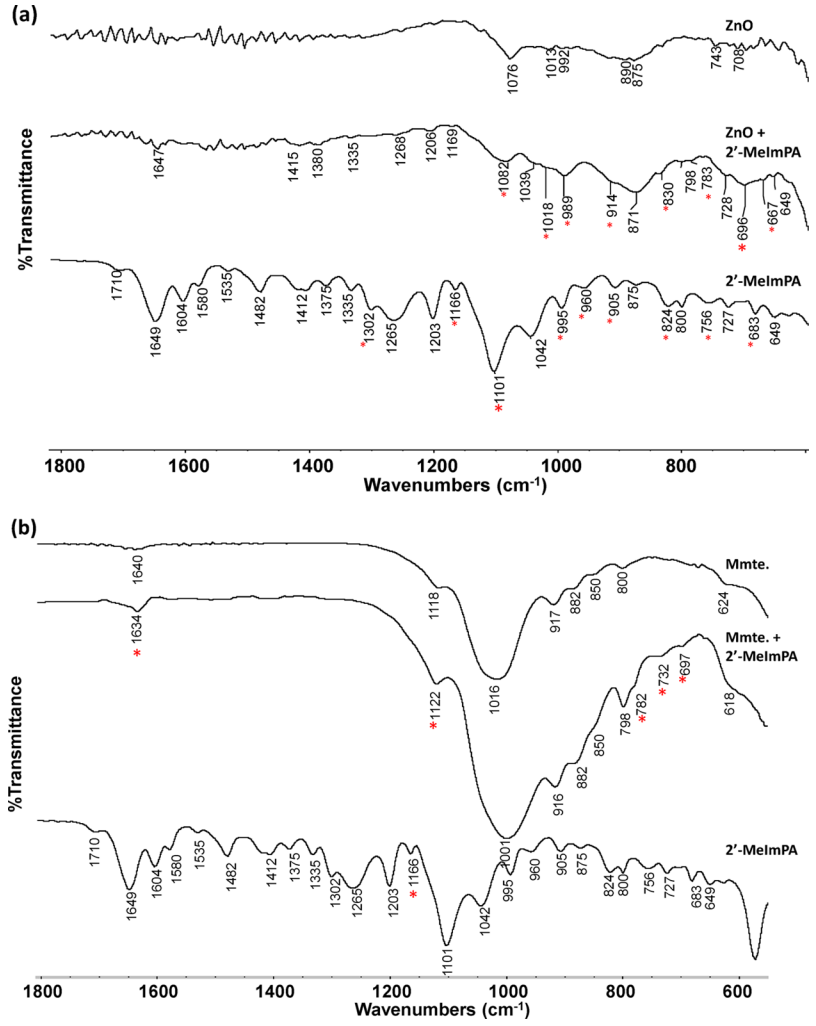

Figure 5. ATR-FTIR spectra of 2-MeImPA adsorbed on minerals in water: (a) zincite and (b) Banin-treated montmorillonite.

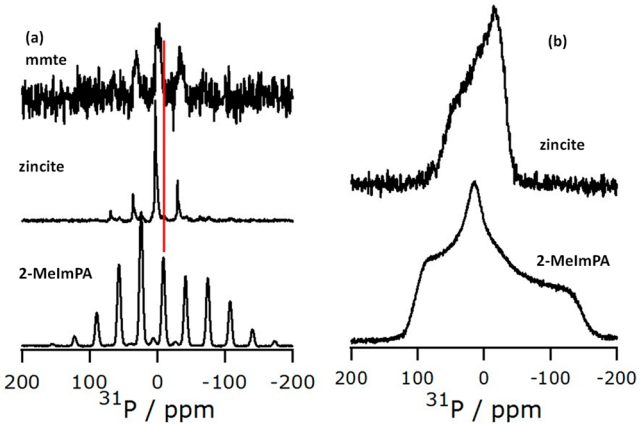

Figure 6. ^{31}P CP NMR spectra of 2-MeImPA. Magic angle spinning spectra (a) of 2-MeImPA in bulk (bottom), adsorbed on zincite (middle), and adsorbed on Banin-treated montmorillonite (top); red solid line indicates ^{31}P chemical shift of 2-MeImPA; and (b) static NMR spectra for 2-MeImPA in bulk (bottom) and adsorbed on zincite (top).

herein (Figure 7). Nucleotides adsorb on montmorillonite through their nitrogenous bases or amine functional group via hydrogen bonding, consistent with the results of molecular dynamics (MD) simulations,[61] thus leaving the phosphate group unconstrained and available for formation of the phosphodiester bond. In contrast, nucleotides adsorb strongly through their phosphate group on positively charged minerals such as zincite, thus making the phosphate unavailable for polymerization. Taken together, our results suggest that adsorption capacity of a mineral is not positively correlated with the catalytic efficiency for polymerization as is widely held in the literature. Rather, detailed molecular-level interactions at the montmorillonite−nucleotides interface are at play wherein the orientation of the phosphate moiety makes it accessible for interaction with another monomer to allow for polymerization.

It is important to note that not all negatively charged minerals catalyze RNA polymerization; indeed, not even all clays are catalysts.[13,20] This suggests that the extent and the nature of isomorphous substitution in the aluminosilicate framework affect the interlayer charge of the clays. Even among the montmorillonites, only certain clays pretreated in a specific manner (the "Banin procedure") showed catalytic properties, and it was conjectured that an acid−base catalysis mechanism involving >OH sites of clay is responsible.[16,17] The >OH sites are found only at the edges of clay platelets, but, in another study from the same research group, the nucleotide was proposed to occupy the interlayer sites of clay[8] (Figure 7). Thus, the precise location of surface sites where polymerization occurs remain unknown. Previous MD simulation results

DOI: 10.1021/acs.jpcc.8b10288
J. Phys. Chem. C 2018, 122, 29386−29397

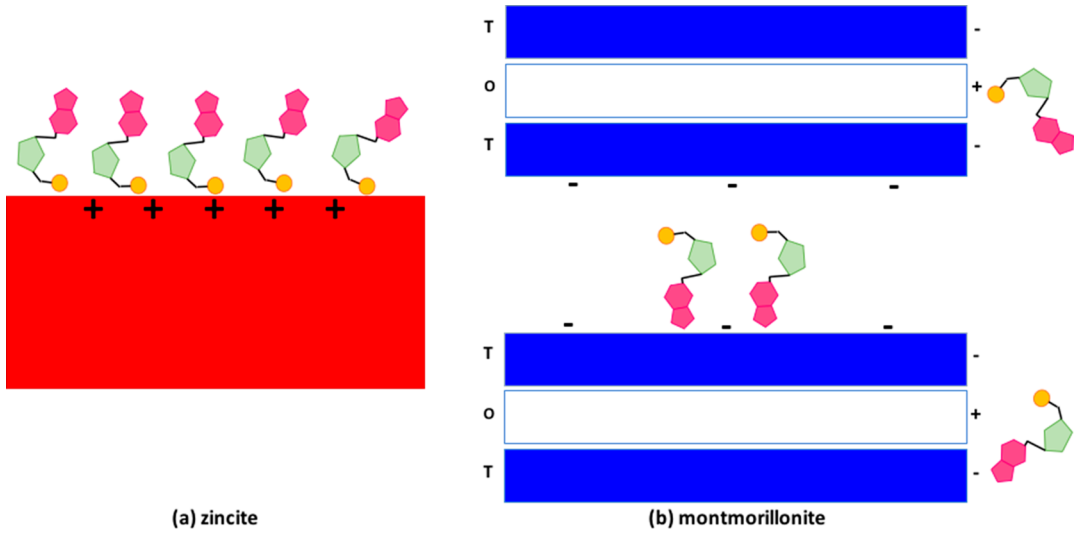

Figure 7. Proposed model for adsorption−polymerization relationship on zincite (a) and montmorillonite (b). On zincite, the phosphate moeity is strongly bonded to mineral surface, thus unavailable for polymerization. On montmorillonite, adsorption on montmorillonite occurs via the nucleobases or amine functional group of the monomer such that the phosphate moeity is accessible to an incoming (or adjacent adsorbed) monomer for polymerization. The schematic is intended only to imply association of the activated nucleotide with the surface. Yellow circle represents 2-methylimidazole phosphate.

suggest a preference of the interlayer sites for polymerization.[61] In summary, the ideal mineral catalyst should allow the phosphate moiety to be available for polymerization while possibly also providing a mechanism for acid−base catalysis. The catalytic role of montmorillonite in this model would be to facilitate the proper alignment of nucleotides, similar to their alignment on a complementary RNA template, as it was originally proposed by Ferris.[14]

We have shown above that, in order to be catalytic to nucleotide polymerization, a mineral must adsorb the nucleotide with the proper conformation where the phosphate remains available for polymerization. Furthermore, we propose that a mineral must also provide a nanoconfined environment in which the activity of water is reduced in order to be catalytic. The decreased activity of water facilitates the elimination of a water molecule between the two nucleotides undergoing polymerization. The ∼1 nm spacing of the interlayer sites of montmorillonite provides such a nanoconfined environment. Thus, montmorillonite fulfills the various requirements for a mineral to be catalytic.

Finally, we address the fact that Banin-treated clays are catalytic, whereas clays treated by simple ion-exchange are not. In the Banin procedure, the clay is washed thoroughly with a strong acid at low pH and then titrated back to pH 7 using NaOH. This ensures thorough removal of all cations from the interlayer sites and results in a pure Na-exchanged clay. The standard ion-exchange process may leave traces of other cations. Taken together, these observations suggest that cations that are strongly hydrated, such as alkali cations or Mg^{2+}, and form outer-sphere ion complexes with the phosphate moiety of the ribonucleotide are permissible in the polymerization reaction. The formation of the ion complex reduces the repulsion between the nucleotide and the negatively charged montmorillonite surface or second nucleotide, while still allowing the cation to be displaced easily by the second nucleotide during the formation of the phosphodiester bond. Other cations, such as Ca^{2+}, which are less strongly hydrated are more easily desolvated and may form inner-sphere complexes with the phosphate moiety of the nucleotide, such that the phosphate is less available for polymerization.

3.8. Role of Magnesium. It was found here that magnesium was not required to achieve short oligomers up to pentamers in the presence of montmorillonite (Figure 3c, Figure 4a). The addition of 10 mM Mg^{2+} promoted the formation of octamers, and oligomer length did not increase up to 100 mM Mg^{2+} (Figure 4). Thus, magnesium plays the role of a cocatalyst to montmorillonite, and a small concentration is as efficient as a much higher concentration. This inference is in agreement with the fact the polymerization up to 10-mers was also achieved at high monovalent alkali cation concentrations (0.8−1.2 M) in the presence of montmorillonite but without any divalent cations present.[19]

Indeed, the formation of up to pentamers in pure water (in the absence of any salts) shown for the first time in the present study indicates that montmorillonite is inherently catalytic (Figure 3c, 4a). The presence of salts aids the polymerization by reducing charge repulsion as the oligomers get longer.

The ability to achieve oligomers even at low magnesium concentrations in the presence of montmorillonite extends the range of geochemical environments in which montmorillonite-catalyzed polymerization may have occurred on early Earth.

Interestingly, 100 mM Mg^{2+} was able to catalyze the formation of up to tetramers (Figure S9) in the absence of montmorillonite though not at lower concentrations. However, such a high concentration of magnesium is implausible in almost any prebiotic geochemical environment.

3.9. Oligomer Length. It is worth noting that only oligomers up to approximately 10-mers have been unambiguously identified in the literature.[5,18,21] One study claimed longer polymers up to about 40-mers,[10] but only gel electrophoresis and HPLC were used in that study without mass spectrometry to confirm the nature of the gel electrophoresis products. In a different approach, it has been stated that unactivated 5′-AMP polymerizes in the presence of lipid molecules during repeated wetting−drying cycles,[53,62,63] and a potential mechanism has been proposed.[64] In these

DOI: 10.1021/acs.jpcc.8b10288
J. Phys. Chem. C 2018, 122, 29386−29397

studies, again, only very short RNA oligomers (<8-mers) have been definitively identified by mass spectroscopy.[53]

The result that only short oligomers are produced nonenzymatically by montmorillonite catalysis has implications for the RNA world theory, where large RNA polymers are assumed to have played the role of both informational and catalytic molecules. Clearly, obtaining such large polymers remains a challenge in the origins of life field. On the other hand, conversion of nonfunctional short RNA strands to functional RNA by primer extension has been recently demonstrated,[2] so it is possible that very long polymers of RNA are not required. However, obtaining even oligomers as long as the original[2] template has currently not been shown nonenzymatically.

4. CONCLUSIONS

In summary, the results presented in the present work indicate that greater adsorption of nucleotides on minerals does not necessarily lead to increased polymerization. Rather, the orientation of the monomers at the mineral/water interface is critical, where the phosphate moiety should be available for polymerization. Magnesium appears not to be essential for oligomerization but acts, rather, as a cocatalyst in the presence of Banin-treated montmorillonite. Short oligomers were obtained even in pure water in the absence of any salts. The present results allow us to propose that at least three properties of a mineral must be fulfilled in order for it to be catalytic in nucleotide polymerization. The mineral must adsorb the mononucleotide in the proper orientation where phosphate is still available for formation of the phosphodiester bond, a nanoconfined environment (e.g., the interlayer sites of montmorillonite) which promotes the dehydration reaction between two nucleotides, and outer sphere complexation of cations (e.g., Mg^{2+} or high alkali cations) with the phosphate moiety of the nucleotide, so that the cation can be easily displaced to form the phosphodiester bond. In the absence of any mineral, up to tetramers were obtained in the presence of 100 mM Mg^{2+}. Finally, obtaining long RNA polymers remains an open challenge in the origins of life field. The results of the present study help resolve an open question for three decades as to what makes a mineral catalytic toward activated ribonucleotide polymerization and should help the narrow the search for other catalytic minerals among the thousands of known minerals.

■ ASSOCIATED CONTENT

Supporting Information

The Supporting Information is available free of charge on the ACS Publications website at DOI: 10.1021/acs.jpcc.8b10288.

Table S1; supplementary Figures S1−S9 (PDF)

■ AUTHOR INFORMATION

Corresponding Author

*E-mail: sahai@uakron.edu.

ORCID

Toshikazu Miyoshi: 0000-0001-8344-9687

Nita Sahai: 0000-0003-3852-0557

Present Addresses

¶Department of Pharmacology, Stony Brook University, 101 Nicolls Road, Stony Brook, NY, 11794-8651.

□Department of Pharmacological Sciences, Stony Brook University, Stony Brook, NY 11794.

Notes

The authors declare no competing financial interest.

■ ACKNOWLEDGMENTS

N.S. is grateful for financial support from the Simons Foundation Origins of Life Initiative award no. 290359, NSF EAR grant no. EAR-1251479, and "start-up" funds from the University of Akron; T.M. gratefully acknowledges NSF DMR 1708999; C.W. gratefully acknowledges NSFCHE-1808115.

■ REFERENCES

(1) Kaddour, H.; Sahai, N. Synergism and Mutualism in Non-Enzymatic RNA Polymerization. *Life* **2014**, *4*, 598−620.

(2) Adamala, K.; Engelhart, A. E.; Szostak, J. W. Generation of Functional RNAs from Inactive Oligonucleotide Complexes by Non-Enzymatic Primer Extension. *J. Am. Chem. Soc.* **2015**, *137*, 483−489.

(3) Cleaves, H. J., II; Scott, A. M.; Hill, F. C.; Leszczynski, J.; Sahai, N.; Hazen, R. Mineral−Organic Interfacial Processes: Potential Roles in the Origins of Life. *Chem. Soc. Rev.* **2012**, *41*, 5502−5525.

(4) Ferris, J. P.; Ertem, G.; Agarwal, V. Mineral Catalysis of the Formation of Dimers of 5′-AMP in Aqueous Solution: The Possible Role of Montmorillonite Clays in the Prebiotic Synthesis of RNA. *Origins Life Evol. Biospheres* **1989**, *19*, 165−178.

(5) Ferris, J. P.; Ertem, G. Oligomerization of Ribonucleotides on Montmorillonite: Reaction of the 5′-Phosphorimidazolide of Adenosine. *Science* **1992**, *257*, 1387−1389.

(6) Ferris, J. P.; Hill, A. R., Jr; Liu, R.; Orgel, L. E. Synthesis of Long Prebiotic Oligomers on Mineral Surfaces. *Nature* **1996**, *381*, 59.

(7) Ertem, G.; Ferris, J. P. Synthesis of RNA Oligomers on Heterogeneous Templates. *Nature* **1996**, *379*, 238.

(8) Ertem, G.; Ferris, J. P. Formation of RNA Oligomers on Montmorillonite: Site of Catalysis. *Origins Life Evol. Biospheres* **1998**, *28*, 485−499.

(9) Franchi, M.; Ferris, J. P.; Gallori, E. Cations as Mediators of the Adsorption of Nucleic Acids on Clay Surfaces in Prebiotic Environments. *Orig. Life Evol. Biosph.* **2003**, *33*, 1−16.

(10) Huang, W.; Ferris, J. P. Synthesis of 35−40 Mers of RNA Oligomers from Unblocked Monomers. A Simple Approach to the RNA World. *Chem. Commun.* **2003**, 1458−1459.

(11) Huang, W.; Ferris, J. P. One-Step, Regioselective Synthesis of up to 50-Mers of RNA Oligomers by Montmorillonite Catalysis. *J. Am. Chem. Soc.* **2006**, *128*, 8914−8919.

(12) Ferris, J. P. Mineral Catalysis and Prebiotic Synthesis: Montmorillonite-Catalyzed Formation of RNA. *Elements* **2005**, *1*, 145−149.

(13) Miyakawa, S.; Joshi, P. C.; Gaffey, M. J.; Gonzalez-Toril, E.; Hyland, C.; Ross, T.; Rybij, K.; Ferris, J. P. Studies in the Mineral and Salt-Catalyzed Formation of RNA Oligomers. *Origins Life Evol. Biospheres* **2006**, *36*, 343−361.

(14) Ferris, J. P. Montmorillonite-Catalysed Formation of RNA Oligomers: The Possible Role of Catalysis in the Origins of Life. *Philos. Trans. R. Soc., B* **2006**, *361*, 1777−1786.

(15) Joshi, P. C.; Pitsch, S.; Ferris, J. P. Selectivity of Montmorillonite Catalyzed Prebiotic Reactions of D, L-Nucleotides. *Origins Life Evol. Biospheres* **2007**, *37*, 3−26.

(16) Joshi, P. C.; Aldersley, M. F.; Delano, J. W.; Ferris, J. P. Mechanism of Montmorillonite Catalysis in the Formation of RNA Oligomers. *J. Am. Chem. Soc.* **2009**, *131*, 13369−13374.

(17) Aldersley, M. F.; Joshi, P. C.; Price, J. D.; Ferris, J. P. The Role of Montmorillonite in Its Catalysis of RNA Synthesis. *Appl. Clay Sci.* **2011**, *54*, 1−14.

(18) Aldersley, M. F.; Joshi, P. C.; Huang, Y. The Comparison of Hydrochloric Acid and Phosphoric acid Treatments in the Preparation of Montmorillonite Catalysts for RNA Synthesis. *Origins Life Evol. Biospheres* **2017**, *47*, 297−304.

DOI: 10.1021/acs.jpcc.8b10288
J. Phys. Chem. C 2018, 122, 29386−29397

(19) Joshi, P. C.; Aldersley, M. F. Significance of Mineral Salts in Prebiotic RNA Synthesis Catalyzed by Montmorillonite. *J. Mol. Evol.* **2013**, *76*, 371−379.
(20) Ferris, J. P.; Ertem, G. Oligomerization Reactions of Ribonucleotides: The Reaction of the 5′-Phosphorimidazolide of Nucleosides on Montmorillonite and Other Minerals. *Origins Life Evol. Biospheres* **1992**, *22*, 369−381.
(21) Burcar, B. T.; Cassidy, L. M.; Moriarty, E. M.; Joshi, P. C.; Coari, K. M.; McGown, L. B. Potential Pitfalls in Maldi-Tof MS Analysis of Abiotically Synthesized RNA Oligonucleotides. *Origins Life Evol. Biospheres* **2013**, *43*, 247−261.
(22) Bernal, J. D. The Physical Basis of Life. *Proc. Phys. Soc., London, Sect. A* **1949**, *62*, 537.
(23) Sowerby, S. J.; Cohn, C. A.; Heckl, W. M.; Holm, N. G. Differential Adsorption of Nucleic Acid Bases: Relevance to the Origin of Life. *Proc. Natl. Acad. Sci. U. S. A.* **2001**, *98*, 820−822.
(24) Maurel, M.-C.; Leclerc, F. From Foundation Stones to Life: Concepts and Results. *Elements* **2016**, *12*, 407−412.
(25) Wächtershäuser, G. Before Enzymes and Templates: Theory of Surface Metabolism. *Microbiol. Rev.* **1988**, *52*, 452−484.
(26) Biondi, E.; Branciamore, S.; Maurel, M.-C.; Gallori, E. Montmorillonite Protection of an UV-Irradiated Hairpin Ribozyme: Evolution of the RNA World in a Mineral Environment. *BMC Evol. Biol.* **2007**, *7*, S2.
(27) Graf, G.; Lagaly, G. Interaction of Clay Minerals with Adenosine-5-Phosphates. *Clays Clay Miner.* **1980**, *28*, 12.
(28) Holm, N. G.; Ertem, G.; Ferris, J. P. The Binding and Reactions of Nucleotides and Polynucleotides on Iron Oxide Hydroxide Polymorphs. *Origins Life Evol. Biospheres* **1993**, *23*, 195−215.
(29) Winter, D.; Zubay, G. Binding of Adenine and Adenine-Related Compounds to the Clay Montmorillonite and the Mineral Hydroxylapatite. *Origins Life Evol. Biospheres* **1995**, *25*, 61−81.
(30) Perezgasga, L.; Serrato-Díaz, A.; Negron-Mendoza, A.; Gal'N, L. D. P.; Mosqueira, F. Sites of Adsorption of Adenine, Uracil, and Their Corresponding Derivatives on Sodium Montmorillonite. *Origins Life Evol. Biospheres* **2005**, *35*, 91−110.
(31) Plekan, O.; Feyer, V.; Šutara, F.; Skála, T.; Švec, M.; Cháb, V.; Matolín, V.; Prince, K. The Adsorption of Adenine on Mineral Surfaces: Iron Pyrite and Silicon Dioxide. *Surf. Sci.* **2007**, *601*, 1973−1980.
(32) Cleaves, H. J.; Jonsson, C. M.; Jonsson, C. L.; Sverjensky, D. A.; Hazen, R. M. Adsorption of Nucleic Acid Components on Rutile (TiO_2) Surfaces. *Astrobiology* **2010**, *10*, 311−323.
(33) Feuillie, C.; Daniel, I.; Michot, L. J.; Pedreira-Segade, U. Adsorption of Nucleotides onto Fe−Mg−Al Rich Swelling Clays. *Geochim. Cosmochim. Acta* **2013**, *120*, 97−108.
(34) Feuillie, C. c.; Sverjensky, D. A.; Hazen, R. M. Attachment of Ribonucleotides on A-Alumina as a Function of pH, Ionic Strength, and Surface Loading. *Langmuir* **2015**, *31*, 240−248.
(35) Hashizume, H. Adsorption of Nucleic Acid Bases, Ribose, and Phosphate by Some Clay Minerals. *Life* **2015**, *5*, 637−650.
(36) Iqubal, M. A.; Sharma, R.; Kamaluddin. Studies on Interaction of Ribonucleotides with Zinc Ferrite Nanoparticles Using Spectroscopic and Microscopic Techniques. *Karbala International Journal of Modern Science* **2015**, *1*, 49−59.
(37) Pedreira-Segade, U.; Feuillie, C.; Pelletier, M.; Michot, L. J.; Daniel, I. Adsorption of Nucleotides onto Ferromagnesian Phyllosilicates: Significance for the Origin of Life. *Geochim. Cosmochim. Acta* **2016**, *176*, 81−95.
(38) Biondi, E.; Furukawa, Y.; Kawai, J.; Benner, S. A. Adsorption of RNA on Mineral Surfaces and Mineral Precipitates. *Beilstein J. Org. Chem.* **2017**, *13*, 393.
(39) Banin, A.; Lawless, J. G.; Mazzurco, J.; Church, F. M.; Margulies, L.; Orenberg, J. B. pH Profile of the Adsorption of Nucleotides onto Montmorillonite. *Origins Life Evol. Biospheres* **1985**, *15*, 89−101.
(40) Adamala, K.; Szostak, J. W. Nonenzymatic Template-Directed RNA Synthesis inside Model Protocells. *Science* **2013**, *342*, 1098−1100.
(41) Powner, M. W.; Gerland, B.; Sutherland, J. D. Synthesis of Activated Pyrimidine Ribonucleotides in Prebiotically Plausible Conditions. *Nature* **2009**, *459*, 239−242.
(42) Scott, W. G.; Szöke, A.; Blaustein, J.; O'Rourke, S. M.; Robertson, M. P. RNA Catalysis, Thermodynamics and the Origin of Life. *Life* **2014**, *4*, 131−141.
(43) Costanzo, G.; Saladino, R.; Botta, G.; Giorgi, A.; Scipioni, A.; Pino, S.; Di Mauro, E. Generation of Rna Molecules by a Base-Catalysed Click-Like Reaction. *ChemBioChem* **2012**, *13*, 999−1008.
(44) Morasch, M.; Mast, C. B.; Langer, J. K.; Schilcher, P.; Braun, D. Dry Polymerization of 3′, 5′-Cyclic Gmp to Long Strands of RNA. *ChemBioChem* **2014**, *15*, 879−883.
(45) Hashizume, H.; Theng, B. K. Adenine, Adenosine, Ribose and 5′-Amp Adsorption to Allophane. *Clays Clay Miner.* **2007**, *55*, 599−605.
(46) Arora, A. K.; Kamaluddin. Interaction of Ribose Nucleotides with Zinc Oxide and Relevance in Chemical Evolution. *Colloids Surf., A* **2007**, *298*, 186−191.
(47) Clayden, N. J.; Waugh, J. S. Solid State ^{31}P NMR Spectroscopy of 5′-AMP Adsorbed on Zinc-Exchanged Clay. *J. Chem. Soc., Chem. Commun.* **1983**, 292−293.
(48) Fry, R. A.; Kwon, K. D.; Komarneni, S.; Kubicki, J. D.; Mueller, K. T. Solid-State NMR and Computational Chemistry Study of Mononucleotides Adsorbed to Alumina. *Langmuir* **2006**, *22*, 9281−9286.
(49) Sahai, N.; Kaddour, H.; Dalai, P.; Wang, Z.; Bass, G.; Gao, M. Mineral Surface Chemistry and Nanoparticle-Aggregation Control Membrane Self-Assembly. *Sci. Rep.* **2017**, *7*, 43418.
(50) Joyce, G.; Inoue, T.; Orgel, L. Non-Enzymatic Template-Directed Synthesis on Rna Random Copolymers: Poly (C, U) Templates. *J. Mol. Biol.* **1984**, *176*, 279−306.
(51) Costanzo, G.; Pino, S.; Timperio, A. M.; Šponer, J. E.; Šponer, J.; Nováková, O.; Šedo, O.; Zdráhal, Z.; Di Mauro, E. Non-Enzymatic Oligomerization of 3′, 5′cyclic AMP. *PLoS One* **2016**, *11*, No. e0165723.
(52) Šponer, J. E.; Šponer, J. í.; Giorgi, A.; Di Mauro, E.; Pino, S.; Costanzo, G. Untemplated Nonenzymatic Polymerization of 3′,5′cGMP: A Plausible Route to 3′, 5′-Linked Oligonucleotides in Primordia. *J. Phys. Chem. B* **2015**, *119*, 2979−2989.
(53) Mungi, C. V.; Rajamani, S. Characterization of RNA-Like Oligomers from Lipid-Assisted Nonenzymatic Synthesis: Implications for Origin of Informational Molecules on Early Earth. *Life* **2015**, *5*, 65−84.
(54) Angell, C. 100. An Infrared Spectroscopic Investigation of Nucleic Acid Constituents. *J. Chem. Soc.* **1961**, 504−515.
(55) Tsuboi, M. Vibrational Spectra of Phosphite and Hypophosphite Anions, and the Characteristic Frequencies of $PO_3^{-2}$and PO_2^- Groups. *J. Am. Chem. Soc.* **1957**, *79*, 1351−1354.
(56) Morgan, R.; Blout, E. Infrared Spectra and the Structure of Polyriboadenylic Acid. *J. Am. Chem. Soc.* **1959**, *81*, 4625−4629.
(57) Khalil, F. L.; Brown, T. L. Infrared Spectra of Adenosine Triphosphate Complexes in Deuterium Oxide Solution. *J. Am. Chem. Soc.* **1964**, *86*, 5113−5117.
(58) Kundu, J.; Neumann, O.; Janesko, B.; Zhang, D.; Lal, S.; Barhoumi, A.; Scuseria, G.; Halas, N. Adenine− and Adenosine Monophosphate (Amp)− Gold Binding Interactions Studied by Surface-Enhanced Raman and Infrared Spectroscopies. *J. Phys. Chem. C* **2009**, *113*, 14390−14397.
(59) Swoboda, A.; Kunze, G. Infrared Study of Pyridine Adsorbed on Montmorillonite Surfaces. *Clays Clay Miner.* **1964**, *13*, 277.
(60) Theophanides, T.; Tajmir-Riahi, H. Spectroscopic Properties of Metal−Nucleotide and Metal−Nucleic Acid Interactions. In *Spectroscopy of Biological Molecules*; Springer: New York, 1984; pp 137−152.
(61) Mathew, D. C.; Luthey-Schulten, Z. Influence of Montmorillonite on Nucleotide Oligomerization Reactions: A Molecular Dynamics Study. *Origins Life Evol. Biospheres* **2010**, *40*, 303−317.
(62) Rajamani, S.; Vlassov, A.; Benner, S.; Coombs, A.; Olasagasti, F.; Deamer, D. Lipid-Assisted Synthesis of Rna-Like Polymers from Mononucleotides. *Origins Life Evol. Biospheres* **2008**, *38*, 57−74.

DOI: 10.1021/acs.jpcc.8b10288
J. Phys. Chem. C 2018, 122, 29386−29397

(63) Deamer, D. The Role of Lipid Membranes in Life's Origin. *Life* **2017**, *7*, 5.
(64) Toppozini, L.; Dies, H.; Deamer, D. W.; Rheinstädter, M. C. Adenosine Monophosphate Forms Ordered Arrays in Multilamellar Lipid Matrices: Insights into Assembly of Nucleic Acid for Primitive Life. *PLoS One* **2013**, *8*, No. e62810.

DOI: 10.1021/acs.jpcc.8b10288
J. Phys. Chem. C 2018, 122, 29386−29397